Effect of electrolysis conditions on the behaviour of porous alumina in acidic Sn(II) solutions

Arūnas Jagminas*, Svetlana Lichušina, Marija Kurtinaitienė and Eimutis Matulionis

Institute of Chemistry,
A. Goštauto 9,
LT-2600 Vilnius, Lithuania
E-mail: jagmin@ktl.mii.lt

The behaviour of porous anodic oxide film of aluminium, known as porous alumina, has been investigated in various aqueous acidic Sn(II) solutions under potentiostatic sweep, ac, and dc electrolysis conditions. The study was carried out using a potentiodynamic *I vs. E* technique complemented by TEM and scanning electron probe investigations. It has been revealed that, under dc conditions, the hydrogen evolution proceeding at the metal|oxide interface leads to a damage of alumina structure and reduction of Sn^{2+} ions at the damaged sites. The damage of the alumina barrier oxide layer has been attributed to the hydrogen evolution from water molecules within the alumina. This process for alumina grown at 15 V dc in the sulphuric acid solution begins at potentials below –1.3 V, reaching the peak current at about –1.9 V *vs*. Ag|AgCl reference. On the contrary, both the ac electrolysis and the fast potential sweep lead to tin deposition into the alumina pores, commencing from the bottom and dying the alumina. However, only during ac electrolysis the alumina barrier oxide layer is not damaged, although this process takes place at much more negative voltages needed for electrons to pass through the barrier oxide layer.

Key words: porous alumina, ac and dc electrolysis, Sn(II) solutions, voltammetric responses

INTRODUCTION

When aluminium is electrochemically oxidized in aqueous solution of sulphuric, oxalic, phosphoric, or chromic acid, a porous anodic oxide film, known as porous alumina, is formed [1]. Being a material of remarkable hardness [2, 3] and uniform thickness up to 200 μm [4], porous alumina exhibits a uniform array of densely packed hexagonal cells, each containing a cylindrical pore separated from the metal by a thin scalloped barrier oxide layer [1, 5]. The cell size of the porous alumina (inter-pore distance) is linearly dependent on the applied anodizing voltage, U_a, with the proportionality constant 2.7 to 2.25 [6–9]. In most cases, the pore density falls in the range of 10^9–10^{11} pores/cm^2. Moreover, it has been reported that on a high grade, annealed and electropolished aluminium surface [10–12] and under a certain anodizing conditions [13–16] an excellent well-ordered two-dimensional array of pores can be obtained. These highly ordered aluminas have recently been reported to be a typical self-ordered template material [10, 17, 18] for fabrication of nanometer-scale arrays of metals [19–21], oxides [22, 23], semiconductors [24–26], multilayered composites [27, 28] and for a variety of applications in electronic, magnetic and optical devices [29–35].

Due to the inherent rectifying properties of the oxide layer, most works on the deposition of metals and semiconductors into the alumina pores have been carried out using ac electrolysis [36, 37]. According to previous reports [38–40], this is an ideal method to fill alumina pores with another material copying exactly the pore array, colouring oxide layer and producing an array with interesting magnetic [41–43], catalytic [39, 44], and optical [35, 45, 46] properties.

A detailed study of the behaviour of thin porous alumina layers during copper and silver electroplating from more concentrated and acidic solutions by dc electrolysis has been carried out by Gileadi et al. [47, 48]. The main conclusion of these works is that hydrogen evolution at the beginning of dc electrolysis damages the alumina barrier oxide layer in places by the reactions:

$$H_2O + e^- \rightarrow 1/2\ H_2 + OH^- \quad (1)$$

* Corresponding author.

$$AlOOH + OH^- \rightarrow AlO_2^- + H_2O \quad (2)$$

leading to the overall reaction:

$$AlOOH + e^- \rightarrow AlO_2^- + 1/2\ H_2, \quad (3)$$

and that both the copper and silver ions cross this layer at the bottom of the pores by migration to be discharged at the Al surface.

In the present work, cyclic voltammetry, transition electron microscopy (TEM), and an electron probe microanalysis (EPMA) have been employed to analyses the behaviour of porous alumina in acidic Sn(II) solutions usually used for alumina colouring under potential sweep, ac and dc conditions. This is based on the recent observations of the authors [49] that voltammetric responses of anodized aluminium in these solutions differ significantly from those in solutions of other salts. The differences observed manifest themselves in the additional polarization wave in the cathodic region at a few volts characteristic of acidic Sn(II) solutions and having at present no general explanation.

EXPERIMENTAL

Experiments were carried out using 99.5% grade Al foil 0.075 mm thick containing Fe 0.24, Si 0.2, Cu 0.03, Zn 0.02, and Ti 0.01% (trade mark AD 0, Russia) or 99.99% grade Al foil 0.125 mm thick (Goodfellow, Cambridge Ltd.). Aluminium samples (10 × 20 mm) were degreased for 5 min in ethanol, etched in 1.5 M NaOH solution at 60 °C for 60 s, neutralized in 1.5 M HNO_3 solution for 30 s, carefully rinsed with distilled water, and air-dried.

Porous alumina was grown in a stirred 1.53 M H_2SO_4 solution at 18 ± 0.5 °C. The cell potential was set at 15 V and the anodizing was conducted for 34 min. Two Pb sheets were used as cathodes. After formation, the porous alumina was rinsed with flowing distilled water for 120 s and transferred immediately to the solution for the ac or dc treatment.

Sine-wave ac of industrial frequency of 50 Hz at a constant voltage amplitude (U_p) ranging from 10 to 18 V_{rms} was used to deposit tin from acidic 0.01 to 0.1 M $SnSO_4$ solution containing H_2SO_4 (to adjust pH from 0.8 to 1.5). Aluminium or magnesium sulphates were used as supporting electrolytes at a concentration of 0.02 to 0.1 M. To prevent Sn^{2+} ion oxidation, tartaric acid and hydrazine sulphate at a concentration of 0.05 M were used. All solutions were prepared from reagent grade chemicals (Merck) used without further purification, and triply distilled water.

Voltammetric measurements were carried out in a conventional three-electrode one-compartment glass cell, using a PI 50.1 potentiostat-galvanostat equipped with a PR-8 programmer, and a home-made PC-controlled function generator. The cyclic voltammograms $I(E)$ were recorded in the E range of different wideness up to +10 ÷ –18 V, at the potential sweep rate ν of 0.1 to 10 V s^{-1}. A carbon rod was used as the auxiliary electrode and $Ag|AgCl|KCl_{sat.}$ as the reference one connected to the cell through a closed wet ground a stopcock and a Luggin capillary. Prior to using, the solutions were de-aerated by an argon stream for 0.5 h. All the experiments were carried out at room temperature. All potential values are reported on the $Ag|AgCl|KCl_{sat}$ potential scale.

The phase composition of the deposits was investigated by X-ray powder diffraction, using a DRON-2 model diffractometer equipped with a graphite monochromated CuK_α radiation (λ 1.5405 Å) operated at 12 mA and 30 kV. A scanning rate of 0.017° s^{-1} in the 2Θ range from 35 to 70° was used in these measurements.

To investigate the morphology of the oxide|aluminium interface before and after tin deposition, both the alumina layer and Al were dissolved chemically from one side of a surface about 0.5 cm^2 in area in hot 1.5 M NaOH solution and then in 0.5 M solution of bromine in methanol, respectively. The latter solution dissolves aluminium, but it has no effect upon the oxide. The replica taken from the exposed area representing the barrier oxide layer surface that had been previously in contact with the metal substrate was investigated using a TEM 100 transmission electron microscope, operated at an accelerated voltage of 75 kV. The distribution of the tin deposit along the cross-section of the alumina layer was studied applying electron probe microanalysis (EPMA) with a JXA-50A scanning electron microscope.

RESULTS AND DISCUSSION

i(E) plots derived for porous alumina in solutions containing Sn^{2+} ions under potential sweep at the rate $v \geq 0.2$ V s^{-1} are shown in Fig. 1a. It should be noted that these plots differ from those obtained in the solutions of other metal salts [50], for instance, of nickel (Fig. 1b). An additional current peak located in the region of potentials from –1.3 to –2.5 V is observed for all acidic Sn(II) solutions with and without the additives preventing the oxidation of Sn^{2+} ions (for example, tartaric acid, hydrazine salts) [36] and additives such as magnesium or aluminium salts preventing the alumina from the barrier oxide layer breakdown [51]. Variations of i against the cathodic potential can be regarded as a proof that the electrochemical behaviour of the porous alumina template in the acidic Sn(II) solutions

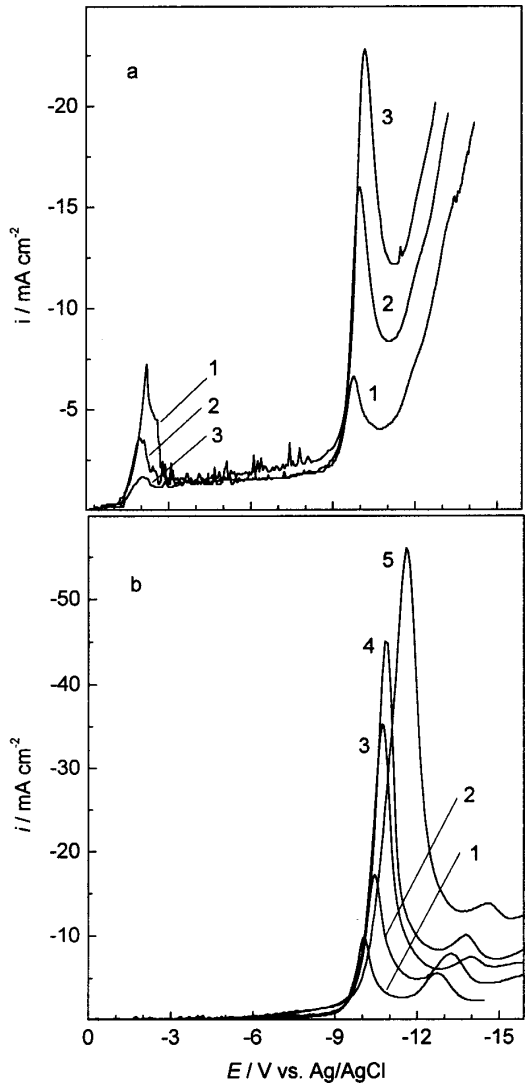

Fig. 1. Potentiodynamic *i(E)* curves showing the electrochemical behaviour of an anodized Al electrode in the solutions: (*a*) $SnSO_4$ 0.1 + tartaric acid 0.05 + hydrazine sulphate 0.05 M + H_2SO_4 up to pH 1.0; (*b*) $NiSO_4$, 0.1 + + H_3BO_3 0.3 + $MgSO_4$ 0.1 M (pH 4.54) at different potential sweep rates v (V s^{-1}): 0.2 (1), 0.4 (2), 0.6 (3), 1.0 (4), and 1.5 (5)

under potential sweep differs substantially in the region of a few volts.

In general, the electrochemical reactions occurring at the porous alumina electrode can take place at the barrier layer at the bottom of the pores or at the aluminium|oxide interface in the sites beneath the pores but not on the outer oxide surface [47]. To gain an insight into whether hydrogen evolution and tin deposition take place at the bottom of the alumina pores or close to the metal|oxide interface, from acidic Sn(II) solution during ac treatment and potential sweep, both scanning electron microscopy (SEM) and transmission electron microscopy (TEM) were employed. The data of microanalysis of tin in the alumina fracture surface obtained after ac treatment or the cathodic potential sweep up to various potentials are displayed in Fig. 2. As shown in Fig. 2a, alternating current electrolysis under voltage control results in tin deposition within the alumina pores commencing from the bottom. For alumina templates grown in the sulphuric acid solution at U_a = 15 V dc the average ac voltage value, U_v, at which tin deposition proceeds varies between 0.35 and 1.3 U_a. An increase in ac electrolysis duration leads to a more complete filling of the alumina pores, resulting in darker bronze tints of alumina layer colouring. Only prolonged ac electrolysis results in the deposition of tin on the top of the film surface.

It has been found that even a single potential sweep in cathodic direction at 10.0 V $s^{-1} \geq v \geq$ 0.2 V s^{-1} up to about –12 V results also in tin deposition at the bottom of the alumina pores (Fig. 2b), dying the film in the same as by ac electrolysis bronze tint. However, the porous alumina is not coloured, if the potential sweep is performed up to a first current peak at about –1.9 V

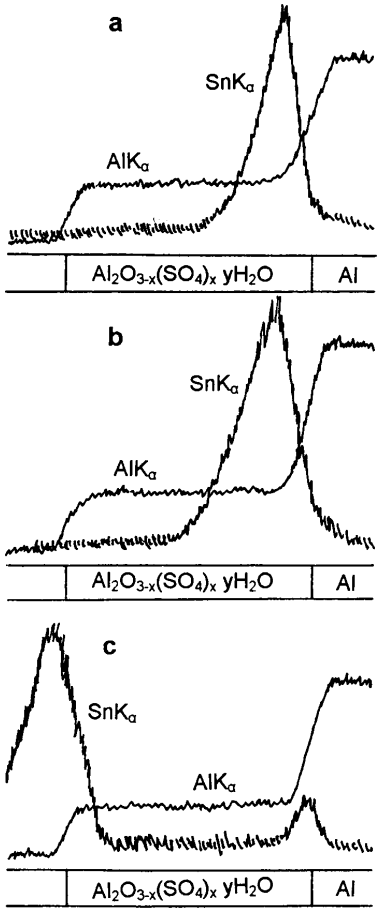

Fig. 2. Line profile of EPMA elemental distribution in a cross-section of the alumina layer after Sn deposition by ac electrolysis at U_p 12 V_{rms} during 8 min (*a*) and after potential sweep at v 0.2 V s^{-1} from E_{st} to –15 V (*b*) or to –1.90 V with further electrolysis at this potential for 2 min (*c*) in solution, as in Fig. 1a

(Fig. 1a). It is also not coloured in the case of dc electrolysis at constant cathodic potentials in the range up to –12 V, although a fast rise of the current is observed from the onset of electrolysis at potentials lower than –2.0 V. A first rise of the current seems to be related to obvious hydrogen evolution and dendritic sponge-like metallic tin deposit growth (Fig. 3) on the top of the alumina surface. However, as is shown in Fig. 2c, the marginal quantity and traces of tin can also be detected at the bottom and in the length of the pores, respectively.

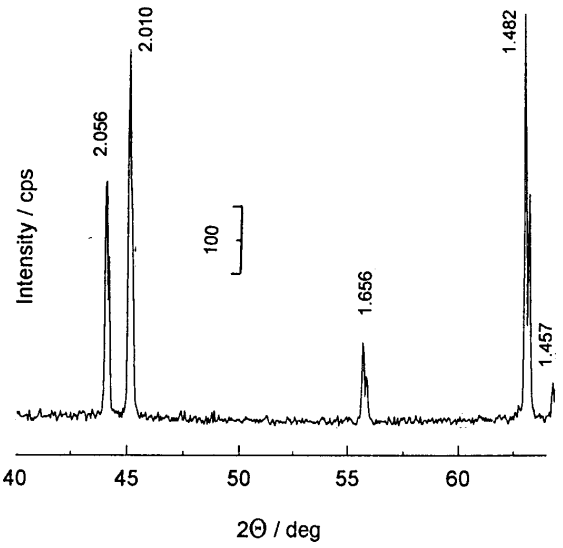

Fig. 3. XRD patterns of sponge-like deposits at the anodized Al electrode surface revealing all distinct lines of metallic tin

It is surprising that a subsequent potential sweep at $v \geq 0.2$ V s^{-1} up to about –12 V performed after a short (up to 3 min) dc electrolysis at the potential of the first current peak of about –1.9 V leads also to the colouring of the alumina layer. However, in this case a sponge-like tin aggregates can also be seen on the alumina surface coloured in bronze. Further, under conditions when the potential is repeated by cycling between ± a few volts relative to E_{st}, the alumina layer is not coloured and only a mushroomed metallic tin growth is observed. These deposits are also spongy, non-adherent and can be easily removed from the electrode surface.

TEM images of the replicas of the aluminium|oxide interface before and after potential sweep, ac and dc treatment of the alumina in acidic Sn(II) solutions were studied and are shown in Fig. 4. The results showed the same scalloped structure (Fig. 4a) of the metal|oxide interface before and after ac electrolysis under voltage control up to $U_v \leq 1.2 \times U_a$ V and $t \leq 10$ min. A similar scal-

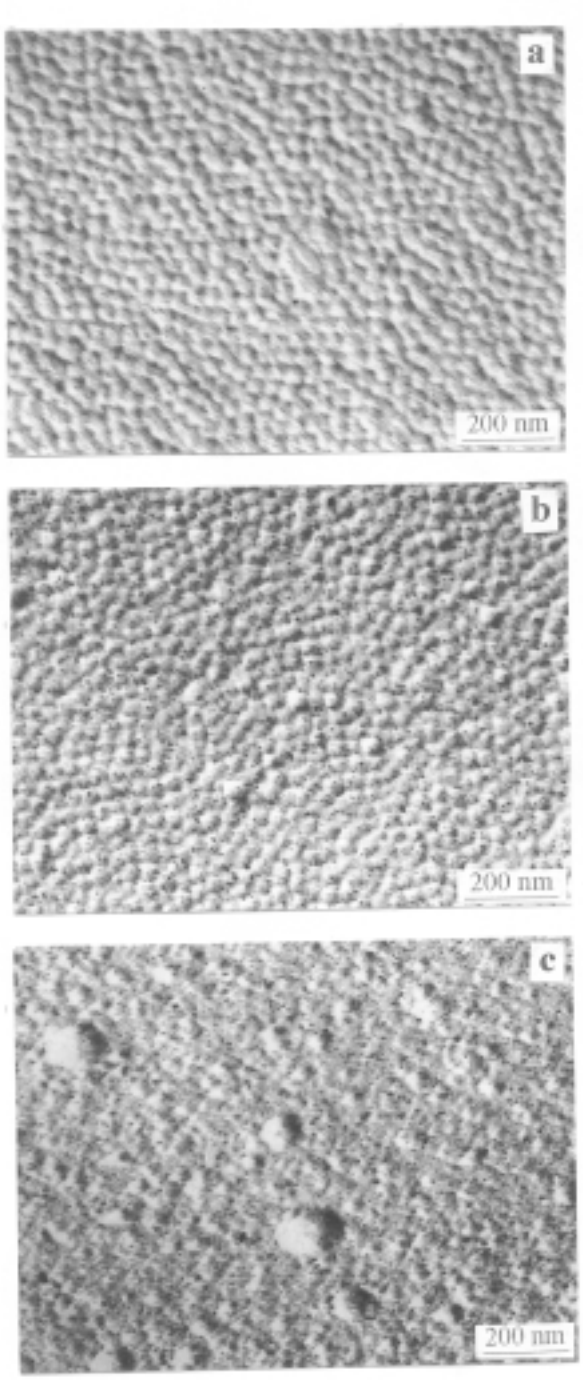

Fig. 4. TEM images showing the structure of the metal¦oxide interface after alumina ac treatment at U_p 12 V_{rms} during 8 min (*a*) and after the potential sweep from E_{st} to –15 V (*b*), or to –1.90 V with further electrolysis at this potential for 2 min (*c*) in solution, as in Fig. 1a

loped structure of the interface is observed after a single potential sweep at $v \geq 0.2$ V s^{-1} up to –15 V. However, in this case a lot of small black spots can be observed on the image from the back side of the barrier layer surface (which has been in contact with the metal), presumably due to the occurrence of narrow pits. It is evident also (Fig. 4c) that dc

electrolysis of the alumina template in acidic Sn(II) solutions even at a few volts favours the damage of the metal|oxide interface structure; it looks like etched without appreciable regularity.

To understand the processes occurring at the bottom of the alumina pores and in the alumina barrier oxide layer during the cathodic potential sweep, *i(E)* plots in different solutions with and without Sn^{2+} ions have been studied. It has been found that the current at potentials below –1.3 V increases rapidly and afterwards the current peak proceeds with fluctuations. In the potential range of the first current wave the current density depends on the composition of the solution, potential sweep rate *v*, and Al purity (Fig. 5) and increases with potential cycling (Fig. 6). Higher current densities were also observed in the cases of more acidic and more concentrated solutions. This current seems to be related to the visible hydrogen evolution. It should be also noted that the current density and the charge consumed for electrochemical reactions at the potentials of the first current wave decrease with an increase in the potential sweep rate (Fig. 1a), indicating that the quantity of the electroactive species to be discharged depends on the electrolysis duration. Again, immersion of the porous alumina in acidic Sn(II) solutions for only a few minutes exerts some influence on the increase in current density and current fluctuations, indicating that chemical dissolution of the porous alumina barrier layer from the outer side in acidic Sn(II) solution also takes place.

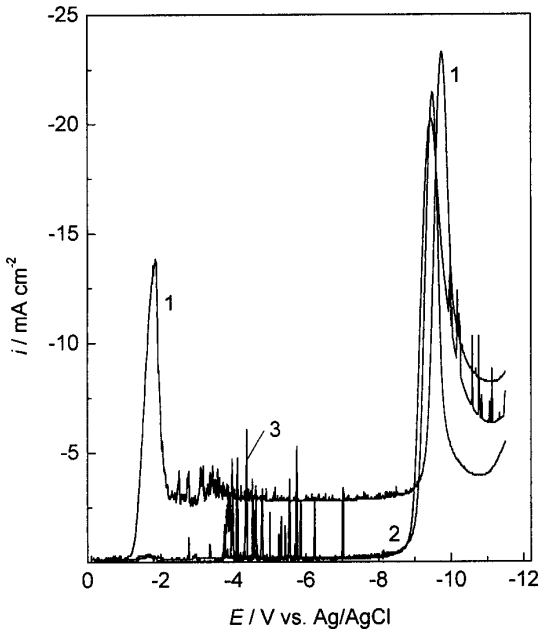

Fig. 5. Potentiodynamic *i(E)* curves at *v* 0.2 V s^{-1} showing the electrochemical behaviour of anodized 99.5% (*1*) and 99.99% (*2, 3*) purity Al electrodes with (*3*) and without (*1, 2*) pretreatment in the acidic (pH 0.8) Sn(II) solution as in Fig. 1a

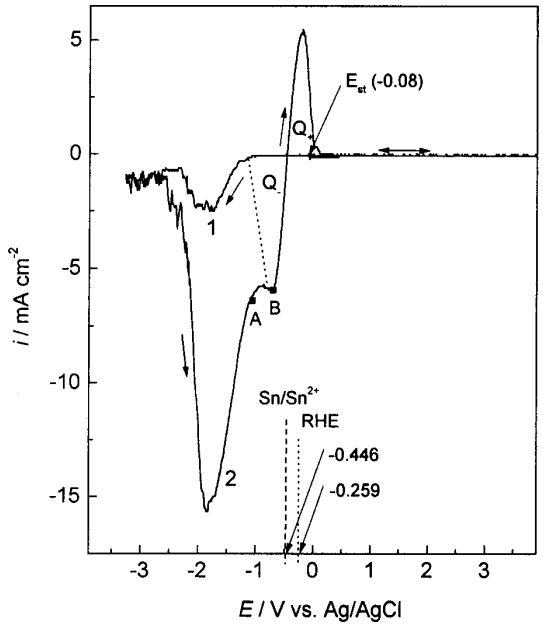

Fig. 6. Potentiodynamic polarization curves at *v* 0.2 V s^{-1} during potential sweep from E_{st} to +3 V and back to –3 V (*1*) and further from –3 V to +3 V (*2*) showing the electrochemical behaviour of an anodized Al electrode in the solution containing (M): $SnSO_4$ 0.1 + tartaric acid 0.05 + hydrazine sulphate 0.05 + H_2SO_4 up to pH 1.0

Typical *i(E)* plots recorded during the first and second potential cycling in acidic Sn(II) solutions in the region of potentials from E_{st} to +3.0 V and further back to –3.0 V are depicted in Fig. 6. During the first potential cycling the current begins to flow only at about –1.30 V, reaching a peak at about –1.90 V. This current seems to be related only to the hydrogen evolution visible to the naked eye. In accordance with [47, 48], the hydrogen evolution can proceed from water molecules (E_{st}^0 –0.828 V) within the alumina as a result of the hydrous nature of the oxide, leading to a damage of the barrier oxide layer by the overall reaction (3). Considering the *i(E)* data obtained during the potential reverse sweep from –3.0 to +3.0 V (curve 2 in Fig. 6), one can see that the hydrogen evolution in this case becomes by one order of magnitude higher than during the former sweep, *i.e.* the higher the degree of the damage of the alumina barrier layer, the higher is the rate of the hydrogen evolution. Moreover, the potential range of the reduction of the electroactive species during reverse sweep expands up to –0.44 V – a potential that is equal to the potential of a $Sn|Sn^{2+}$ redox couple. Further, for the current density in the region of potentials from –1.90 V to about –0.44 V, an obvious delay of the current (AB stretch in Fig. 6) is seen. This feature

could be related to the onset of the reduction of Sn^{2+} ions at the alumina|oxide interface at sites of the partially damaged alumina barrier oxide layer. Based on the literature data considering the transport of cations [47, 48, 52] and anions [53] through the alumina barrier layer during plating and oxide film growth, it was assumed that Sn^{2+} ions are supplied to the reduction place by migration, because the barrier oxide layer of the porous alumina is too thick (about 15 nm) [1, 54] to conduct or to tunnel the electrons through the oxide at a few volts. As a result of tin deposition, the anodic current of tin dissolution is observed on the *i(E)* plots during the subsequent potential sweep in the region from –0.44 to +0.12 V. However, the charge consumed for tin dissolution, Q_+, seems to be somewhat less than the charge consumed for tin deposition, which is expected to be equal to the Q_- area shown in Fig. 6. Eventually this assumption was confirmed by the electrode potential attained at the open-circuit after the cycling and being equal to –0.44 V, which is rather close to the $Sn|Sn^{2+}$ redox couple potential. However, as is clear from the previous data regarding the framework colour, the alumina layer is not coloured during potential sweep between +3 to –3 V. Therefore, it is reasonable to assume that tin deposition takes place only at some sites of the damaged interface beneath the pores and later only in some fraction of the pores, leaving the pores to be mainly inactive. This is consistent with experimental findings on tin incorporation in a cross-section of porous alumina in acidic Sn(II) solutions after a potential sweep was carried out only up to the current peak (about –1.90 V), with subsequent short electrolysis at this potential (Fig. 2c). From the tin traces incorporated along the alumina cross-section it is evident that tin starts growing on the surface of alumina like mushrooms only if some pores have been filled with tin and the metallic contact with the aluminium substrate has been established through tin nanowires having a lower resistance.

Considering the results obtained during the potential sweep, the reasons for such high current densities and the alumina barrier layer damage in acidic Sn(II) solutions at the beginning of the cathodic potential scan are not clear. Moreover, it is rather difficult to explain why the reduction reactions are inhibited at higher cathodic potentials. The current-potential curves obtained under the same experimental conditions in acidic solutions with and without Sn^{2+} ions are shown in Fig. 7. It is obvious that *i(E)* plots recorded in these solutions mostly differ in the regions of the potentials of the first and second current peaks at about –2.0 and below –10.5 V, even though their pH are rather close. As can be seen from curve 2 in Fig. 7, the current density in

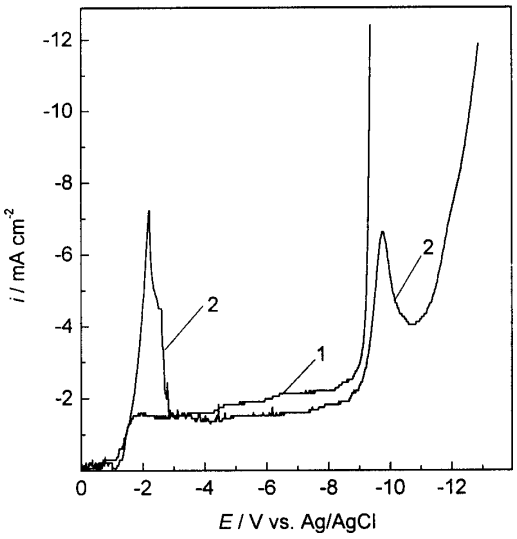

Fig. 7. The same as in Fig. 6 at v 0.2 V s^{-1} in acidic (pH 0.9) solution of H_2SO_4 (*1*) and in the solution, containing (M): $SnSO_4$ 0.1 + tartaric acid 0.05 + hydrazine sulphate 0.05 + H_2SO_4 up to pH 0.9 (*2*)

the solutions containing Sn^{2+} ions at potentials close to about –2.2 V is significantly higher, indicating that both hydrogen evolution and Sn^{2+} ion discharge processes take place simultaneously. In accordance with [47, 48] and the data obtained here, it seems likely that tin ions can readily cross the alumina barrier oxide layer at the bottom of the pores by migration under the influence of a high electric field to be discharged at the aluminium|oxide interface at the sites of reduced barrier layer. However, this process seems to take place only in a lesser fraction of the pores, since the alumina layer is not coloured and only traces of tin were incorporated in the alumina cross section. In addition, the amount of tin is larger at the metal|oxide interface than along the alumina cross-section (Fig. 2c), implying that tin deposition begins and proceeds irregularly. The decrease in the current density during the further potential sweep in the cathodic direction seems to be related only to the hindering of tin deposition, since the charges consumed for hydrogen evolution in the range of potentials from about –3.0 to –8.5 V in the solutions with and without Sn^{2+} ions are very close. The second current peak observed close to the potential of about –10.5 V in the solutions with and without Sn^{2+} ions differs markedly. This current peak observed in aqueous acidic solutions without any metal ions has been related [55] to the formation of surface complexes with a charge carrier at the metal|oxide interface due to the reaction of the oxide film with water molecules hindering hydrogen evolution at more negative potentials. Thus, it can be suggested that Sn^{2+} ions show an activating influence on the formation of such

complexes. Further experiments are needed to confirm this hypothesis.

CONCLUSIONS

The behaviour of porous anodic oxide film of aluminium known as porous alumina has been investigated in various aqueous acidic Sn(II) solutions under potentiostatic sweep, ac, and dc electrolysis conditions. The study was carried out using a potentiodynamic *I vs*. *E* technique complemented by TEM and scanning electron probe investigations. It has been revealed that, under dc conditions, the hydrogen evolution proceeding at the metal|oxide interface leads to a damage of alumina structure and reduction of Sn^{2+} ions at the damaged sites. The damage of the alumina barrier oxide layer has been attributed to the hydrogen evolution from water molecules within the alumina. This process for alumina grown at 15 V dc in the sulphuric acid solution begins at potentials below –1.3 V reaching the peak current at about –1.9 V *vs*. Ag|AgCl reference. On the contrary, both the ac electrolysis and the fast potential sweep lead to tin deposition into the alumina pores, commencing from the bottom and dying the alumina. However, only during ac electrolysis the alumina barrier oxide layer is not damaged, although this process takes place at much more negative voltages needed for electrons to pass through the barrier oxide layer.

ACKNOWLEDGEMENT

The authors are indebted to Dr. Remigijus Juškėnas from the Institute of Chemistry, Vilnius, Lithuania for the performance of X-ray diffraction measurements.

Received 20 January 2003
Accepted 11 February 2003

References

1. F. Keller, M. S. Hunter and D. L. Robinson, *J. Electrochem. Soc.*, **100**, 411 (1953).
2. N. G. Chechenin, J. Bottiger and J. P. Krog, *Thin Solid Films*, **261**, 219 (1995).
3. M. Maejima, K. Saruwatari, K. Isawa and M. Takaya, *Hyomen Gijutsu*, **48**, 230 (1997).
4. R. C. Furneaux, W. R. Rigby and A. P. Davidson, *Nature*, **337**, 147 (1989).
5. J. P. O'Sullivan and G. C. Wood, *Proc. Roy. Soc. London*. **A317**, 511 (1970).
6. T. Takahashi and N. Nagayama, *J. Chem. Soc. Jpn*., **36**, 34 (1968).
7. K. Ebihara, T. Takahashi and N. Nagayama, *J. Metal Surf. Fin. Soc. Jpn*., **34**, 548 (1983).
8. A. P. Li, F. Müller, A. Birner, K. Nielsch and U. Gösele, *J. Appl. Phys*., **84**, 6023 (1998).
9. A. Jagminas, D. Bigelienė, I. Mikulskas and R. Tamošiūnas, *J. Cryst. Growth*, **233**, 591 (2001).
10. H. Masuda, F. Hasegawa and S. Ono, *J. Electrochem. Soc*., **144**, L127 (1997).
11. H. Masuda, K. Yada and A. Osaka, *Jpn. J. Appl. Phys*., **37**, L1340 (1998).
12. O. Jessensky, F. Müller and U. Gösele, *J. Electrochem. Soc*., **145**, 3735 (1998).
13. H. Masuda and M. Satoh, *Jpn. J. Appl. Phys*., **35**, L126 (1996).
14. D. Allmawlawi, K. A. Bosnick, A. Osika and M. Moskovits, *Adv. Mater*., **12**, 1252 (2000).
15. H. Masuda, H. Yamada, M. Satoh, H. Asoh, M. Nakao and T. Tamamura, *Appl. Phys*. *Lett*., **71**, 2770 (1997).
16. H. Masuda, H. Asoh, M. Watanabe, K. Nishio, M. Nakao and T. Tamamura, *Adv. Mater*., **13**, 189 (2001).
17. H. Masuda and K. Fukuda, *Science*, **268**, 1466 (1995).
18. O. Jessensky, F. Müller and U. Gösele, *Appl. Phys. Lett*., **72**, 1173 (1998).
19. S. Kawai and R. Ueda, *J. Electrochem. Soc*., **122**, 32 (1975).
20. H. Masuda, K. Nishio and N. Baba, *Thin Solid Films*, **223**, 1 (1993).
21. C. R. Martin, R. Parthasarathy and V. Menon, *Electrochim. Acta*, **39**, 1309 (1994).
22. S. Ishida and S. Ito, *J. Met. Fin. Soc. Jpn*., **40**, 1394 (1999).
23. Y. Ishikawa and Y. Matsumoto, *Electrochim. Acta*, **46**, 2819 (2001).
24. P. Hoyer and H. Masuda, *J. Mater. Sci. Lett*., **12**, 1228 (1996).
25. J. D. Klein, R. D. Herrick, I. D. Palmer and M. J. Sailor, *Chem. Mater*., **5**, 902 (1993).
26. D. Routkevitch, T. Bigioni, M. Moskovits and J. M. Xu, *J. Phys. Chem*., **100**, 14037 (1996).
27. L. Piraux, J. M. George, J. F. Despres, C. Leroy, E. Ferain, R. Legras, K. Ounadjela and A. Fert, *Appl. Phys. Lett*., **65**, 2484 (1994).
28. P. R. Evans, G. Yi and E. Schwarzacher, *Appl. Phys. Lett*., **76**, 481 (2000).
29. C. G. Granqvist, A. Anderson and O. Hundri, *Appl. Phys. Lett*., **35**, 268 (1979).
30. R. J. Tonucci, B. L. Justus, A. J. Campillo and C. E. Ford, *Science*, **258**, 783 (1992).
31. T. M. Whitney, J. S. Jiany, P. C. Searson and C. L. Chien, *Science*, **261**, 1316 (1993).
32. C. A. Huber, T. E. Huber, M. Sadogi, J. A. Lubin, S. Manalis and C. B. Prater, *Science*, **263**, 800 (1994).
33. C. R. Martin, *Science*, **266**, 1961 (1994).
34. G. Schmid, M. Baumle, M. Geerkens, I. Heim, C. Osemann and T. Sawitowski, *Chem. Soc. Rev*., **28**, 179 (1999).
35. K. Preston and M. Moskovits, *J. Phys. Chem*., **97**, 8495 (1993).
36. E. Herrmann, *Galvanotechnik*, **B 63**, 110 (1972).
37. H. Masuda, H. Tanaka and N. Baba, *Bull. Chem. Soc. Jpn*., **66**, 305 (1993).
38. I. Clebny, B. Doudin and J.-Ph. Ansermet, *Nanocryst. Mater.*, **2**, 637 (1993).
39. D. G. W. Goad and M. Moskovits, *J. Appl. Phys*., **49**, 2929 (1978).
40. K. Douglas, G. Devaud and N. A. Clark, *Science*, **257**, 642 (1992).

41. S. Kawai and I. Ishiguro, *J. Electrochem. Soc*., **123**, 1047 (1975).
42. D. All-Mawlawi, N. Coombs and M. Moskovits, *J. Appl. Phys*., **70**, 4421 (1991).
43. D. J. Dunlop, S. Xu, Ö. Ördemir, D. All-Mawlawi and M. Moskovits, *Phys. Earth Planet. Inter*., **76** 113 (1993).
44. M. Miller and M. Moskovits, *J. Am. Chem. Soc*., **111**, 9250 (1989).
45. M. Saito, M. Kirihara, T. Taniguchi and M. Miyagi, *Appl. Phys. Lett*., **55**, 607 (1989).
46. M. J. Tierney and C.R. Martin, *J. Phys. Chem.*, **93**, 2878 (1989).
47. J. Gruberger and E. Gileadi, *Electrochim. Acta*, **31**, 1531 (1986).
48. A. Zagiel, P. Natishan and E. Gileadi, *Elecrtochim. Acta*, **35**, 1019 (1990).
49. V. Skominas, S. Lichušina, P. Miečinskas and A. Jagminas, *Trans. IMF*, **79**, 213 (2001).
50. A. Jagminas, S. Lichusina, M. Kurtinaitiene and A. Selskis, *Appl. Surf. Sci.* (in press).
51. A. Jagminas, *J. Appl. Electrochem*. **32**, 1201 (2002).
52. G. Patermarakis and K. Moussoutzanis, *Electrochim. Acta*, **40**, 699 (1995).
53. K. Shimizu, H. Habazaki, P. Skeldon, G. E. Thompson and G. C. Wood, *Electrochim. Acta*, **45**, 1805 (2000).
54. G. Patermarakis, P. Lenas, C. Karavassilis and G. Papayiannis, *Electrochim. Acta*, **36**, 702 (1991).
55. E. K. Oshe and O. N. Markova, *Zaschita Met*., **32**, 239 (1996).

A. Jagminas, S. Lichušina, M. Kurtinaitienė, E. Matulionis

ELEKTROLIZĖS SĄLYGŲ ĮTAKA AKYTO ALUMINA ELGSENAI RŪGŠČIUOSE SN(II) TIRPALUOSE

S a n t r a u k a

Tirta aliuminio anodinių oksidinių plėvelių (alumina), užaugintų sieros rūgšties tirpaluose (U_a 15 V), elgsena rūgščiuose vandeniniuose Sn(II) tirpaluose potencialo skleidimo, kintamosios ir nuolatinės srovių sąlygomis. Greta elektrocheminių atlikti metalas|oksidas ribos mikrostruktūros ir nusodinamo alavo sudėties bei pasiskirstymo plėvelėje tyrimai. Nustatyta, kad nuolatinės srovės elektrolizės metu metalas|oksidas riboje skiriasi vandenilis. Vandenilio redukcija iš vandens, esančio alumina sudėtyje, suardo oksido barjerinį sluoksnį metalas|oksidas riboje ir sąlygoja alavo kristalizaciją. Šis procesas prasideda, esant –1.3 V, ir pasiekia ribos srovę, esant –1.9 V potencialų vertėms. Tiek kintamosios srovės, tiek katodinio potencialo greito skleidimo metu alavas nusėda aliuminio oksido matricos akučių dugne, nuspalvindamas oksidinę plėvelę bronzine spalva. Tačiau oksido barjerinis sluoksnis nesuardomas tik kintamosios srovės elektrolizės metu, nors alavo jonų redukcijai šiuo atveju reikia gerokai neigiamesnių potencialų, būtinų tuneliuoti elektronams per barjerinį sluoksnį.